

Dynamic response of target electrons on elastic scattering cross sections for heavy-ion impact on a high- Z atom

Yasushi Hoshino and Yoshiaki Kido*

Department of Physics, Ritsumeikan University, Kusatsu, Shiga-ken 525-8577, Japan

(Received 17 September 2002; revised manuscript received 30 December 2002; published 24 July 2003)

Large-angle elastic scattering cross sections were measured for medium energy He^+ and Ne^+ ions impact on Ni, Sb, and Hf atoms and the results are compared with those calculated using screened interatomic potentials. As the screened Coulomb potential, we employed the Molière, Ziegler-Biersack-Littmark (ZBL), and that calculated numerically by solving the Poisson equation applied to the Hartree-Fock (HF) atomic model. For He^+ impact, the ZBL and HF (He^{2+} is assumed) potentials reproduced well the observed scattering cross sections but the Molière potential underestimated them significantly. Surprisingly, however, for Ne^+ impact on Sb and Hf, the observed scattering cross sections were much larger than those calculated from all the above screened interatomic potentials, although Ne^{10+} was assumed for the HF potential. In a large-angle collision, a projectile heavy ion attracts the target electrons to distort the electron cloud and as a result it changes the electric field upon the projectile. The observed scattering cross sections are reproduced well by assuming a simple model that the center of gravity of the target electrons slightly shifts toward the projectile by 0.09–0.12 Å for Hf and 0.066–0.070 Å for Sb from the nucleus.

DOI: 10.1103/PhysRevA.68.012718

PACS number(s): 34.20.Cf, 34.50.Fa

Ion scattering spectroscopy has been widely employed for elemental depth profiling and structure analysis of solid surfaces. The quantitative analysis is made by classical mechanics based on the simple binary collision model, so-called “Rutherford backscattering (RBS)” analysis. In the low- and medium-energy regimes (several hundreds of eV—a few hundreds of keV; however, the screening of a nuclear charge by the bound electrons must be taken into account. Up to now, several screened Coulomb potentials have been proposed [1–4] and the most frequently used are the Molière and Ziegler-Biersack-Littmark (ZBL) potentials. It has been recognized that the Molière potential gives significantly different values of shadow cone radii in the low-energy regime and the improved one is the ZBL potential, which is applicable to all the energy regimes [5].

The screened interatomic potentials proposed so far have basically a static nature. In a real large-angle collision, target electrons should respond to the electric field induced by an incident projectile charge and thus the response should depend upon the ion energy and its trajectory. The elastic scattering of slow electrons from atoms and molecules has some resonant characters [6,7] which have been discussed in terms of polarization of a target atom and molecule [8–10]. In ion-atom collisions, the observed ionization cross sections of the target and projectile were discussed, considering the nuclear (projectile)–electron (target) (screening) and the electron–electron interaction (antiscreening) [11,12]. To our knowledge, however, there is no report on the calculations of elastic scattering cross sections affected by the response of target electrons to projectiles in ion-atom collisions.

In this study, we show that a heavy ion impact distorts the electron cloud of a target atom and it changes the elastic

scattering cross sections. The differential scattering cross sections were measured with a surface-barrier-type detector for 70–130 keV He^+ ions incident on Ni ($Z_2=28$), Sb ($Z_2=51$), and Hf ($Z_2=72$) and for 90, 110, and 130 keV Ne^+ impact on Sb and Hf. Polycrystalline Ni (32.8 Å) and amorphous HfO_2 (7.2, 8.5, and 19.2 Å) layers were formed on oxidized Si substrates by molecular beam epitaxy (MBE) and on oxynitrided Si substrates by chemical vapor deposition (CVD), respectively. Reflective high-energy electron diffraction (RHEED) confirmed polycrystallinity of the Ni layer and cross-sectional transmission electron microscopy (TEM) showed amorphous and uniform HfO_2 growth on Si(001). In addition, the Si(111)- $\sqrt{3}\times\sqrt{3}$ -Sb surface was also prepared as a sample. We measured in advance the absolute amounts of Ni, Sb, and Hf by RBS using 2.0 MeV He^+ beams. The accelerated ion beams were collimated to $0.06\times 2\text{ mm}^2$ and impinged on the target, which was mounted on a six-axis goniometer. The typical beam current was a few nA and the irradiation area was shifted after an ion dose of 0.1 μC . Therefore, the sputter erosion of the target layers was negligibly small. The backscattered He and Ne particles were detected with a bakable surface-barrier-type solid state detector (SSD), which was mounted on a turn table. This SSD has an insensitive layer of Au with thickness 100–150 Å deposited on an n -type Si(001) substrate. The transmission rate for 80 keV Ne particles was estimated to be about 95% from Monte Carlo simulation, using the TRIM code [13]. The backscattering experiment was performed *in situ* for the Ni/Si(111) and Si(111)- $\sqrt{3}\times\sqrt{3}$ -Sb and *ex situ* for the HfO_2 /Si(001) under an ultrahigh vacuum condition ($\leq 3\times 10^{-10}$ Torr). In order to measure the beam current precisely, we applied a bias voltage of +90 V to the target and also to a final aperture placed in front of the target. The accuracy of the integrated beam current was estimated to be better than $\pm 5\%$, which was confirmed by comparing the target beam current with that measured by a well-designed Faraday cup placed in front of the scattering chamber.

*Corresponding author. FAX: +81-77-561-2657;
email address: ykido@se.ritsumei.ac.jp

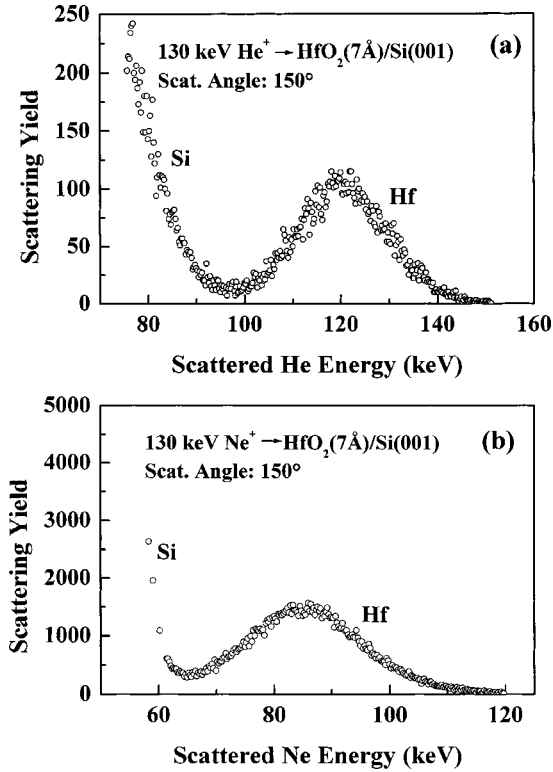


FIG. 1. Backscattering spectra observed for 130 keV He^+ (a) and Ne^+ (b) ions incident on $\text{HfO}_2(7.2 \text{ \AA})/\text{Si}(001)$ and backscattered to 150° .

Figures 1(a) and 1(b) show the backscattered spectra observed for 130 keV He^+ and Ne^+ ions, respectively, incident on $\text{HfO}_2(7.2 \text{ \AA})/\text{Si}(001)$ and backscattered to 150° . For Ne^+ impact, the scattering component from Hf slightly overlaps with that from Si. The contribution from the overlapping region was evaluated by computer-simulated spectrum analysis [14]. Thus, the total backscattering yields were obtained with an accuracy of 3–4%. The spectrum broadening, in particular, seen for Ne^+ impact is due to the passage through the insensitive Au layer of the surface barrier detector. The backscattering yield is simply given by

$$Y = Q \left(\frac{d\sigma}{d\Omega} \right) \Delta\Omega N \Delta x, \quad (1)$$

where Q , $d\sigma/d\Omega$, $\Delta\Omega$, and $N\Delta x$ are, respectively, the number of ions incidence evaluated from the integrated beam current, differential scattering cross section of interest, solid angle subtended by the detector, and target thickness (atoms/cm²). Q , $\Delta\Omega$, and $N\Delta x$ are already known and thus the measurement of the scattering yield Y gives the corresponding scattering cross section.

Figure 2(a) shows the observed scattering cross sections for 90, 110, and 130 keV He^+ ions incident on Ni and backscattered to 110° . We calculated the scattering cross sections using four types of interatomic potentials: (1) unscreened, (2) Molière, (3) ZBL, and (4) HF potentials. The HF potential called here was calculated numerically by solving the following Poisson equation:

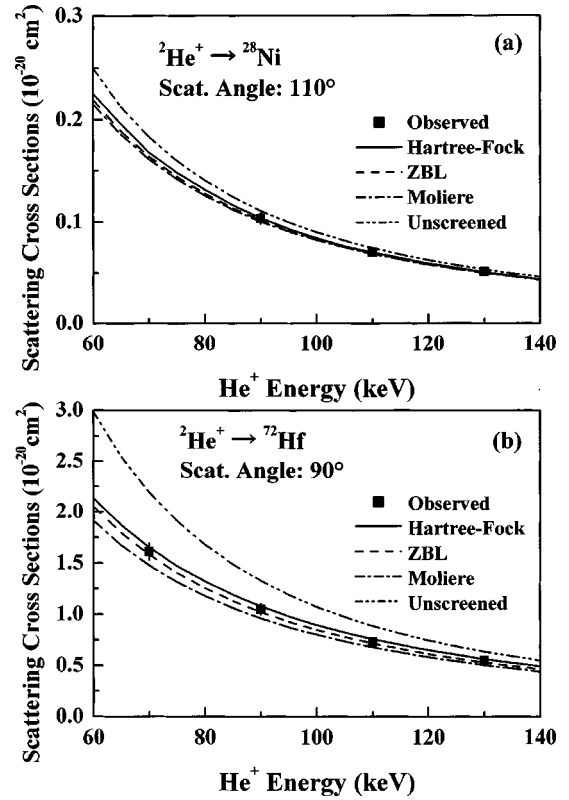


FIG. 2. Observed (full squares) and calculated scattering cross sections for He^+ impact on Ni (a) and on Hf (b) as a function of incident energy. Calculated scattering cross sections are denoted by solid (HF), dashed (ZBL), dot-dashed (Molière), and dot-dot-dashed (unscreened) curves.

$$\nabla^2 V(r) = 4\pi e \rho_e(r) - 4\pi Z_2 e \delta(r), \quad (2)$$

where e and Z_2 are the elemental charge and target Z number, respectively, and $\rho_e(r)$ is the electron density calculated numerically from the Hartree-Fock-Slater model [15,16]. It must be noted that all the conventional interatomic potentials such as Molière and ZBL include no (effective) projectile charge explicitly and are expressed only by internuclear distance and screening radius given by Z_1 (projectile Z number) and Z_2 . The HF potential presented here needs an effective projectile charge to act as an interatomic potential. We calculated numerically the ion trajectories by computer simulation (to solve the equation of motion at a time interval $\Delta t = 10^{-19}$ s) for impact parameters s and $s + \Delta s$ and obtained the corresponding scattering angles θ and $\theta - \Delta\theta$. Then the scattering cross section ($d\sigma/d\Omega$) is given by $2\pi s \Delta s / 2\pi \sin \theta \Delta\theta$. The observed scattering cross sections agree well with those calculated from the above three types of screened interatomic potentials and are slightly smaller than the Rutherford scattering cross sections (unscreened Coulomb potential). Here, the He^{2+} state was assumed for the HF potential. In the present scattering conditions, the distance of the closest approach ranges from 0.0068 to 0.0095 Å, which is considerably smaller than the average radius of Ni $1s$ orbit. This situation gives a small screening effect. Figure 2(b) shows the observed and calculated scat-

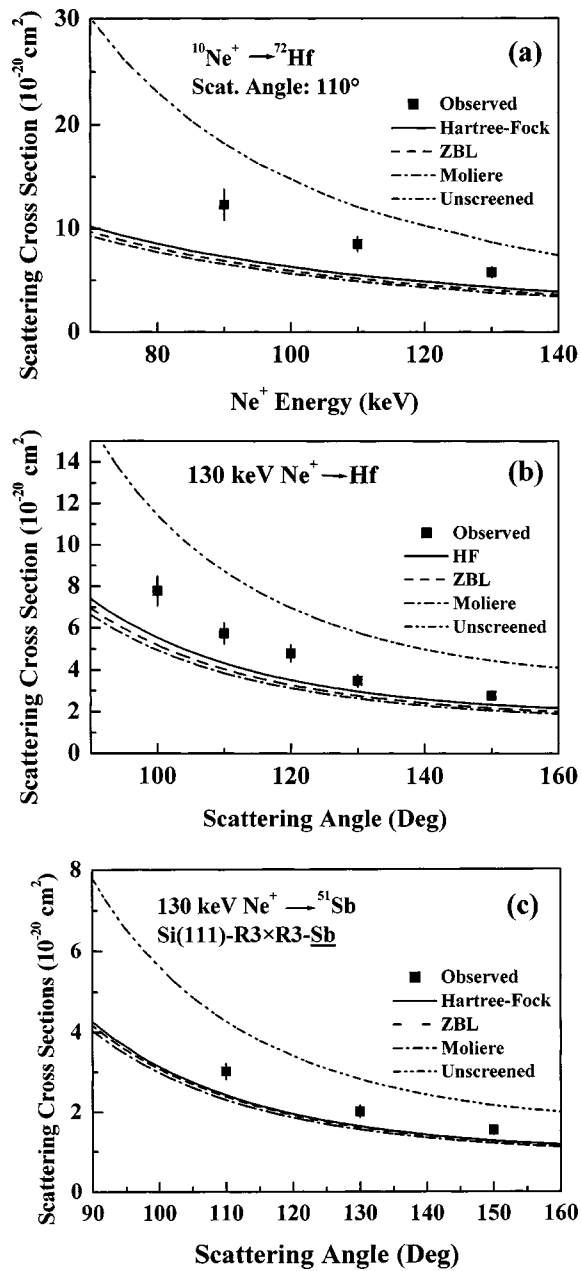


FIG. 3. Observed (full squares) and calculated scattering cross sections for 90, 110, and 130 keV Ne^+ impact on Hf and backscattered to 110° (a) and for 130 keV Ne^+ impact on Hf and backscattered to 100° – 150° (b). Calculated scattering cross sections are depicted with the same symbols denoted in Fig. 2.

tering cross sections for 70, 90, 110, and 130 keV He^+ ions incident on Hf and backscattered to 90° . The observed scattering cross sections are in good agreement with those calculated using the ZBL and HF potentials. However, the Molière potential gives slightly smaller values. In fact, the ZBL potential is the improved version of the Molière potential, which is approximated to the Thomas-Fermi potential. Apparently, the Thomas-Fermi potential fails in the region far from and too close to a nucleus. The ZBL potential was optimized to get overall agreement with realistic potential calculations over several hundreds of ion-target combination.

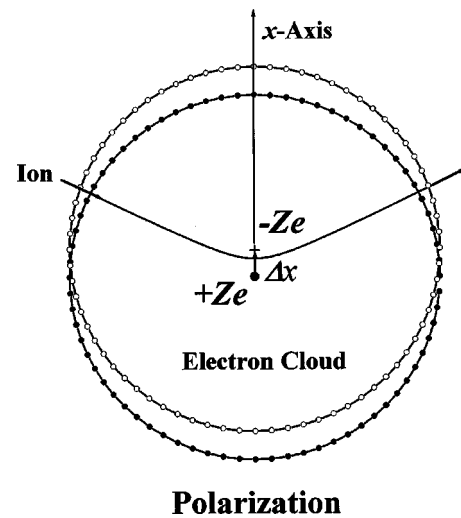


FIG. 4. Schematic of an ion trajectory and a shift (Δx) of electron cloud along the symmetry axis x of elastic scattering in the center-of-mass (c.m.) system.

The present result reflects the fact that the distance of closest approach is extended over a range from 0.019 to 0.036 Å in the above scattering conditions, which is considerably larger than the average radius of Hf 1s orbit and thus the projectile He ions experience the potential screened significantly by the inner electrons.

Figure 3(a) shows the scattering cross sections for 110 and 130 keV Ne^+ ions backscattered to 110° from Hf. The observed scattering cross sections are much larger than those calculated from all the screened interatomic potentials but smaller than the Rutherford scattering cross sections. Here, the Ne^{10+} state was assumed for the HF potential and thus it gives a maximum scattering cross section calculated from screened Coulomb potentials. Figure 3(b) indicates the observed and calculated scattering cross sections for 130 keV

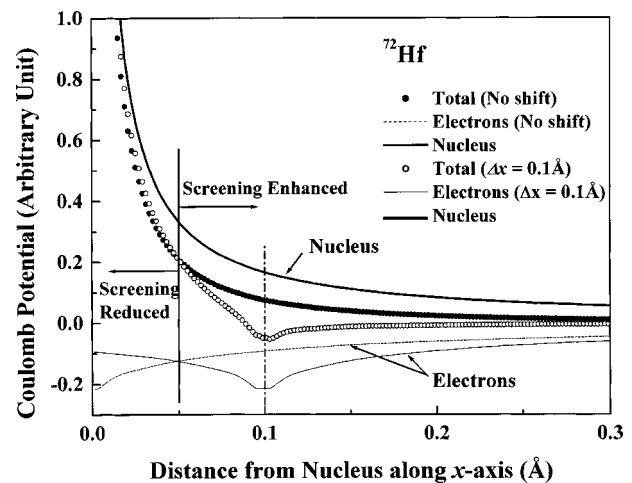


FIG. 5. Coulomb potentials generated by the Hf-nucleus (solid curve) and its bound electrons distributed spherically as a function of the distance from the nucleus along the symmetry axis x . The full and open circles denote the total potentials calculated assuming (i) $\Delta x=0$ and (ii) $\Delta x=+0.1 \text{ \AA}$, respectively (see Fig. 4).

TABLE I. Observed elastic scattering cross sections (10^{-20} cm²), shift of center of gravity of bound electrons [Δx (Å)], distance of closest approach (Å) and collision time (Δt fs) as a function of scattering angle or incident energy. In the case of He⁺ impact, the values of Δx were not estimated, because the observed scattering cross sections agree with those calculated from the potentials of ZBL and HF (He²⁺).

130 keV Ne ⁺ incident on Hf					
	100°	110°	120°	130°	150°
$d\sigma/d\Omega$ (10^{-20} cm ²)	7.8 ± 0.7	5.75 ± 0.5	4.8 ± 0.4	3.9 ± 0.4	2.9 ± 0.3
Δx (Å)	0.115 ± 0.01	0.110 ± 0.01	0.115 ± 0.01	0.091 ± 0.01	0.090 ± 0.01
r_{\min} (Å)	0.060	0.0584	0.0571	0.0560	0.0546
Δt (10^{-15} s)	0.0344	0.0346	0.0348	0.0350	0.0353
Ne ⁺ → Hf: scattering angle = 110°					
	90 keV		110 keV		130 keV
$d\sigma/d\Omega$ (10^{-20} cm ²)	12.3 ± 1.5		8.5 ± 0.7		5.75 ± 0.5
Δx (Å)	0.14 ± 0.02		0.12 ± 0.01		0.11 ± 0.01
r_{\min} (Å)	0.0749		0.0654		0.0583
Δt (10^{-15} s)	0.0484		0.0402		0.0346
130 keV Ne ⁺ incident on Sb					
	110°		130°	150°	
$d\sigma/d\Omega$ (10^{-20} cm ²)	3.08 ± 0.3		2.06 ± 0.2	1.57 ± 0.2	
Δx (Å)	0.066 ± 0.008		0.069 ± 0.008	0.070 ± 0.009	
r_{\min} (Å)	0.0583		0.0473	0.0456	
Δt (10^{-15} s)	0.0298		0.0301	0.0305	
He ⁺ incident on Hf: scattering angle = 90°					
	70 keV	90 keV	110 keV	130 keV	
$d\sigma/d\Omega$ (10^{-20} cm ²)	1.61 ± 0.15	1.05 ± 0.10	0.73 ± 0.06	0.55 ± 0.05	
Δx (Å)					
r_{\min} (Å)	0.017	0.0199	0.0235	0.029	
Δt (10^{-15} s)	0.0143	0.0110	0.0088	0.0073	

Ne⁺ impact on Hf as a function of scattering angle. Also in this case, the observed scattering cross sections are substantially larger than those calculated from the screened potentials. Here, we must note that the distance of closest approach ranging from 0.057 to 0.065 Å is considerably larger than the mean radii of Hf 1s, 2s, and 2p orbits. Similar enhancement of the scattering cross sections was also observed for Ne⁺ impact on Sb atoms. The observed scattering cross sections for 130 keV Ne⁺ ions scattered from Sb to 110°, 130°, and 150° are about 30% larger than those calculated using the screened potentials, as shown in Fig. 3(c).

What diminishes the screening of the target nucleus for Ne⁺ impact on Hf and Sb? The multiple scattering would increase seemingly the observed scattering cross sections. This contribution appears for path length exceeding a critical thickness and then increases with increase in path length in a medium. In the case of HfO₂ layers, the critical thickness was estimated experimentally to be about 25 Å by varying the emerging angle scaled from the surface plane at a fixed scattering angle. Only one possible event is a distortion of the electron cloud of the target atom, which is induced by Ne⁺ impact. It changes the electric field upon the projectile

and thus changes its trajectory. In comparison with the He⁺ impact, the projectile electronic charge and the closest distance for the Ne⁺ impact are five- and threefold, respectively, and conversely the Ne velocity is almost one-third of the He velocity. The time lapse during a large-angle collision of Ne⁺ → Hf is about 0.05 fs, which is ten times as long as that of the He⁺ → Hf collision. Thus, the bound electrons of Hf would be strongly attracted to the projectile Ne nucleus and thus it changes the electric field upon the projectile. As a most probable event during such a large-angle collision, a quasimolecular state is formed and it also distorts the electron clouds. In any sense, a redistribution of the target electrons changes the ion trajectories and as a result the elastic scattering cross section is also changed. Now, we propose a simple model that the center of gravity of the bound electrons shifts by Δx from the target nucleus along the symmetry axis of the elastic scattering without changing the spherical symmetry. This situation is illustrated in Fig. 4. The target electrons are shifted toward the symmetry axis x due to time-averaged attractive force. It must be noted that this assumption is not very realistic but useful to evaluate quantitatively the extent of the distortion (redistribution) of the electron cloud.

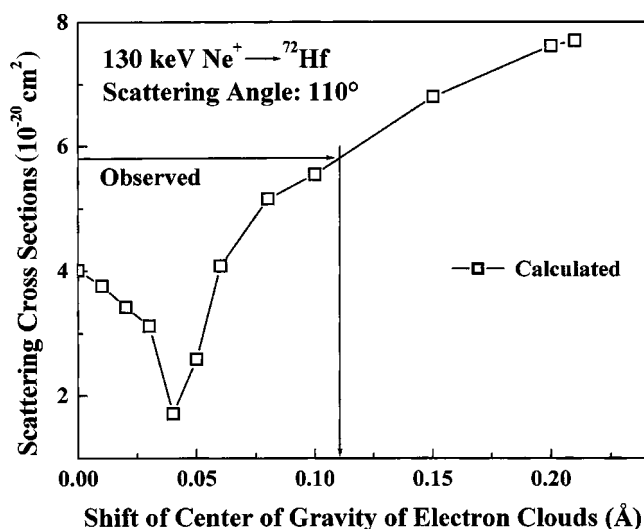


FIG. 6. Differential scattering cross sections for 130 keV Ne^+ ions backscattered to 110° from Hf as a function of shift (Δx) calculated using the HF potential (Ne^{10+} was assumed). The arrows indicate the observed scattering cross section and the corresponding shift.

Figure 5 shows the Coulomb potentials generated by the Hf nucleus and the bound electrons as a function of the distance from the Hf nucleus along the x axis (symmetry axis of elastic scattering in the center-of-mass (c.m.) frame, see Fig. 4). Here, we assumed two cases: (i) no shift ($\Delta x=0$) and (ii) a shift of $+0.1$ Å along the x axis. In case (ii), it is seen that the screening of the nuclear charge is enhanced or reduced for the positions larger or smaller than a critical value of 0.05 Å. The differential scattering cross sections for 130 keV Ne^+ ions backscattered to 110° from Hf were calculated as a function of Δx and are shown in Fig. 6. It indicates that the scattering cross section first decreases with increase in Δx up to 0.04 Å and then increases rapidly. Such a behavior is basically expected from Fig. 5. A shift of 0.11 ± 0.01 Å (Δx) reproduces well the observed scattering cross section ($5.76 \times 10^{-20} \text{ cm}^2$). All the observed scattering cross sections are

well reproduced assuming the shift of 0.09 – 0.12 Å for Hf and 0.066 – 0.070 Å for Sb (see Table I). It is seen that the Δx value depends significantly on Z_2 and projectile energy and slightly on the distance of closest approach and collision time Δt . Unfortunately, we find no simple universal relation as a function of the above parameters. As exact description of the distortion of electron clouds, an adiabatic treatment such as quasimolecular formation would be possible. It is strongly required to deduce some scaling law for enhanced scattering cross sections as a function of Z_1 , Z_2 , incident energy, and distance of closest approach.

In summary, we measured the differential scattering cross sections for 70 – 130 keV He^+ and Ne^+ ions incident on Ni, Sb, and Hf and backscattered to 60° – 150° with the surface-barrier-type SSD. The observed scattering cross sections for He^+ impact on Ni, Sb, and Hf are in good agreement with those calculated, using the ZBL- and HF-type screened interatomic potentials. The Molière potential reproduces well the scattering cross sections for He^+ impact on Ni but significantly underestimates those for the Sb and Hf targets. In the case of Ne^+ impact on Sb and Hf, the scattering cross sections measured are substantially enhanced compared with those calculated from the screened Coulomb potentials (Molière, ZBL, HF). The observed scattering cross sections are reproduced well assuming the simple model that the center of gravity of the bound electrons shifts by 0.09 – 0.12 Å for Hf and 0.066 – 0.070 Å for Sb along the symmetry axis of elastic scattering in the c.m. frame. It means that the electron cloud of the target atom is distorted by the attractive force of the projectile nucleus. During a large-angle collision, a quasimolecular state is probably formed and the resultant redistribution of the electron cloud acts as a kind of polarization. The present study clearly shows the fact that conventional interatomic potentials are no longer valid for a medium-energy heavy ion impact on a high- Z atom. In such a case, a dynamical response of the target electrons to the incident projectile must be taken into account.

This work was supported by the Grant-in-aid for Scientific Research of the Ministry of Education, Science and Culture, Japan.

-
- [1] J. Lindhard, M. Scharff, and H. E. Schiøtt, K. Dan. Vidensk. Selsk. Mat. Fys. Medd. **33**, 14 (1963).
 [2] K. B. Winterbon, P. Sigmund, and J. B. Sanders, K. Dan. Vidensk. Selsk. Mat. Fys. Medd. **37**, 14 (1970).
 [3] W. D. Wilson, L. G. Hagmark, and J. P. Biersack, Phys. Rev. B **9**, 2458 (1977).
 [4] J. F. Ziegler, J. P. Biersack, and W. Littmark, *The Stopping and Range of Ions in Matter* (Pergamon, New York, 1985).
 [5] H. J. Kang, E. Kawatoh, and R. Shimizu, Jpn. J. Appl. Phys., Part 2 **23**, L262 (1984).
 [6] W. Sohn, K.-H. Kocher, K.-M. Scheuerlein, K. Jung, and H. Ehrhardt, J. Phys. B **19**, 3625 (1986).
 [7] J. C. Gibson, M. A. Green, K. W. Trantham, S. J. Buckman, P. J. O. Teubner, and M. J. Brunger, J. Phys. B **32**, 213 (1999).
 [8] A. Temkin, Phys. Rev. **116**, 358 (1959).
 [9] J. Callaway, R. W. LaBahn, R. T. Pu, and W. M. Duxler, Phys. Rev. **168**, 12 (1968).
 [10] T. N. Rescigno, D. A. Byrum, W. A. Isaacs, and C. W. McCurdy, Phys. Rev. A **60**, 2186 (1999).
 [11] J. H. McGuire, N. Stolterfoht, and P. R. Simony, Phys. Rev. A **24**, 97 (1981).
 [12] E. C. Montenegro, W. S. Melo, W. E. Meyerhof, and A. G. de Pinho, Phys. Rev. A **48**, 4259 (1993).
 [13] J. F. Ziegler, J. P. Biersack, and W. Littmark, *The Stopping and Range of Ions in Matter* (Pergamon, New York, 1985).
 [14] Y. Kido and T. Koshikawa, J. Appl. Phys. **67**, 187 (1990).
 [15] E. Clementi and C. Roetti, At. Data Nucl. Data Tables **14**, 177 (1974).
 [16] A. D. McLean and R. S. McLean, At. Data Nucl. Data Tables **26**, 197 (1981).